BNL-71024-2003-BC



To : SUWARNO
Fr : G.P.S

Chapter 3

# The Dynamics of Hydrogen Atom Abstraction from Polyatomic Molecules

XIANGHONG LIU and ARTHUR G. SUITS

*Chemistry Department, Brookhaven National laboratory, Upton, NY 11973 and Department of Chemistry, Stony Brook University, Stony Brook, NY 11794*

## Contents

## 1 Introduction

The hydrogen atom abstraction reaction is an important fundamental process that is extensively involved in atmospheric and combustion chemistry. The practical significance of this type of reaction with polyatomic hydrocarbons is manifest, which has led to many kinetics studies.[1–4] The detailed understanding of these reactions requires corresponding dynamics studies. However, in comparison to the A + HX → AH + X reactions, the study of the dynamics of A + HR → AH + R reactions is much more difficult, both experimentally and theoretically (here and in the following, A stands for an atom, X stands for a halogen atom, and R stands for a polyatomic hydrocarbon radical). The complication stems from the *structured* R, in contrast to the *structureless* X. First of all, there are many internal degrees of freedom in R that can participate in the reaction. In addition, there are different carbon sites from which an H atom can be abstracted, and the dynamics are correspondingly different; there are also multiple identical carbon sites in HR; and in the picture of a local reaction, there exist competitions between neighboring H atoms, and so on. Despite this complexity, there have been continuing efforts to obtain insight into the dynamics of these reactions. In this chapter, some examples are presented, including the reactions of ground state H, Cl, and O atoms, with particular focus on our recent work using imaging to obtain the differential cross sections for these reactions.

In Sec. 2, we will briefly review H atom abstraction from alkanes by hot H atoms, i.e. H + HR → $H_2$ + R. Valentini and coworkers have conducted extensive studies on this class of reactions.[5–7] These studies are essentially carried out under single collision conditions in bulk, and the rovibrational state populations of the $H_2$ product are measured. Based on observations with a series of alkane reagents, they have developed some models of energy

disposal to understand the dynamics and to predict the dynamics of systems not yet studied, even without knowledge of the details of the potential energy surface (PES).

In Sec. 3, we will review previous studies on reactions of Cl + alkanes. The experimental methods used fall into two categories. One is the "photoloc" approach, in which the HCl product is probed by resonance enhanced multiphoton ionization (REMPI), its internal energy distribution is obtained, and the differential cross section is derived by simulation of the ion time-of-flight (TOF) spectrum. The other category is crossed molecular beam study; the alkyl radical product is probed by VUV single photon ionization and its neutral TOF spectra at different angles in the laboratory frame are measured; by simulation of the TOF spectra, the center-of-mass (CM) frame angular distribution and translational energy release spectrum are obtained.

We will focus at length in Secs. 4 and 5 on the Cl + alcohols and O + alkanes reactions respectively. These studies combined the crossed molecular beam technique with velocity map imaging (VELMI) using VUV single photon ionization "universal" detection of the hydrocarbon radical products, which we believe are the most direct measurement of the CM differential cross section. In the experimental part of Sec. 4, we also present some results concerning the VUV single photon ionization probe technique, addressing the question whether there is strong dependence of the detection efficiency on the internal energy of the hydrocarbon radical. This issue is also relevant to the studies on Cl atom reactions in Secs. 3 and 4.

vacuum ultraviolet (VUV

## 2 H + HR → $H_2$ + R Reactions

Valentini's group has studied this class of reactions extensively. In addition to the atom – diatom series H + HX → $H_2$ + X (X = Cl, Br, I),[8] they studied alkane reactions, including the target molecules $CD_4$, $C_2H_6$, $C_3H_8$, $n$-$C_5H_{12}$, and $n$-$C_6H_{14}$.[5–7] Owing to the complexity of the HR molecules, Valentini's group tried to understand and predict the dynamics from the aspects of kinematics, thermochemistry, and the structure of HR. Their concern is mainly focused on the rovibrational state distribution of the $H_2$ product, because this is what they measure directly.

The details of their experimental setup can be found in Ref. 9, and here we only give a brief description. A mixture of HI (20 torr) and HR (vapor pressure) was expanded through a 0.8 mm diameter nozzle to generate a

molecular beam. 19 mm downstream of the nozzle, the molecular beam was crossed by a loosely focused 266 nm laser beam. This photolysis pulse produces translationally hot **H** atoms, which react with the alkane to form $H_2$. After a short photolysis-probe delay of 10–30 ns, which was chosen to assure single collision conditions, the $H_2$ products were state selectively detected by REMPI.

They observed that only few of the energetically accessible states of the $H_2$ product were measurably populated, and this was interpreted as the result of a kinematic restraint on the product translational energy.[5] A positive correlation of rotational and vibrational excitation was observed, i.e. the rotational excitation became higher for higher vibrational state of the product. This correlation became stronger with increasing size of the alkane molecule.

In their previous studies[10,11] of the reactions of $H + HX \rightarrow H_2 + X$, they found in the QCT calculations that the local H–H impact parameter $b_{H-H}$ was the crucial factor that governed the dynamics, and this "localized collision" model was able to quantitatively account for the opacity functions extracted from the QCT calculations, as well as the experimentally measured rotational distribution and reaction cross sections. The local H–H impact parameter was defined as the distance between the relative velocity vector and a line parallel to it that passes through the abstracted H atom.

quasiclassical trajectory (QCT

For the H + HR reactions, the local reaction model was extended. The model postulates that reactant structure influences the $H_2$ product rotational distribution through two effects. The first is a modification of the opacity function, a consequence of the existence of multiple identical reaction sites that compete for the reaction. This modification is mainly a truncation of the maximum impact parameter, for there is overlap of the acceptance cone of neighboring H atoms and the reaction will occur at the smaller $b_{H-H}$ with the presence of the reaction barrier and the angular dependence of the barrier height. In consequence, this effect reduces the yield of higher rotational states because of the correlation between $b_{H-H}$ and the rotational quantum number $j'$. The second effect is a relaxation of the otherwise tight coupling between the constraints of the total angular momentum conservation and the total energy conservation because the polyatomic product with small rotational constants serves as an energetically "cheap" sink for angular momentum. This uncoupling should facilitate the production of higher $H_2$ rotational states at small total angular momentum.

The effect of truncation of the opacity function is more pronounced in $v' = 0$ than $v' = 1$; for $v' = 1$, the smaller cone of acceptance contributing to $H_2$ product makes competition from alternative neighboring sites less likely. On the other hand, the effect of uncoupling between the constraints of total angular momentum and total energy is expected to act more effectively for $v' = 1$ than $v' = 0$, because for producing $v' = 1$, the collision occurs at small impact parameters where angular momentum is more easily transferred to the radical product and the collision would otherwise be angular momentum limited. This effect results in the positive correlation between the vibrational and rotational excitations observed in the $H_2$ product. Furthermore, as the length of the alkyl chain increases, the impulsive energy release as the products separate will lead to increasing radical rotational excitation, and the effect of uncoupling is expected to show up more. These expectations have also been observed in their experiments.

## 3 Cl + HR → HCl + R Reactions

### 3.1 *Introduction*

Hydrogen atom abstraction by chlorine atoms from small alkanes has been investigated in detail recently under single collision conditions using REMPI probe of the HCl products and core extracted ion TOF methods.[12–17] These experiments took advantage of the anisotropic distribution of Cl photofragments in the photodissociation of the $Cl_2$ to generate Cl reactants with a well known velocity and angular distribution. The photolysis light is 355 nm, the third harmonic output of the Nd : YAG laser. The probe laser was fired after a delay, which is usually ~100 ns, chosen to allow the reaction products build up and at the same time ensuring single collision conditions. The REMPI ionization of HCl product provides the nascent rovibrational state distribution and analysis of the core extracted ion TOF profiles leads to laboratory velocity distributions. With assumptions about the CM speed distribution, CM angular distributions can be obtained. Zare and coworkers[12–14] and Dagdigian and coworkers[15–17] have used these methods to measure state selected differential cross sections for the HCl products in the reactions of Cl with a number of saturated hydrocarbons from methane to isobutane. These are briefly summarized in Secs. 3.2–3.4. More recently, Suits and coworkers studied Cl + propane/pentane reactions by using molecular beam technique with the hydrocarbon radical probed

by vacuum ultraviolet (VUV) synchrotron radiation ionization.[18,19] These studies are summarized in Sec. 3.5.

## 3.2 Cl + Methane

The reaction of the Cl with methane in its ground vibrational state is slightly endothermic with an activation barrier ca. 2–3 kcal/mol. At a collision energy of 3.7 kcal/mol, only HCl ($v = 0$) is accessible and the rotational population was found to be very cold.[12] The HCl product was scattered exclusively in the backward direction in the CM frame with respect to the incident Cl atom. In the hard sphere collision model, strong back-scattering is correlated with small impact parameters "$b$". This angular distribution can be intuitively explained within the line-of-centers model[20] where only the collisions with small $b$ lead to sufficient energy along the reaction coordinate to overcome the reaction barrier.

The reaction of Cl with vibrationally excited methane ($v_3 = 1$, asymmetric stretch) at the same collision energy showed remarkably different behavior.[13] The total cross section is increased dramatically, and the dynamics are significantly different. The additional available energy provided by excitation of the methane reactant makes the reaction to produce HCl ($v = 0$, $J$) exothermic by ca. 7 kcal/mol and opens up the HCl ($v = 1$, $J$) product channel, which is endothermic by ca. 2 kcal/mol. The HCl ($v = 0$) products were backward scattered in analogy to the reaction with methane in its ground vibrational state, but showed greater rotational excitation. This was interpreted as the consequence of similar reaction mechanism in both cases and a greater acceptance cone for the case of methane $v_3 = 1$. The reactant vibrational energy provides some available energy along the reaction coordinate; this lessens the energy that must be provided by the relative translation, and increases the range of impact parameters leading to reactions. The HCl ($v = 1$, $J$) products were found to have lower rotational excitation than the HCl ($v = 0$, $J$) products and exhibited very different scattering. For very low $J$ HCl ($v = 1$, $J$) products, the scattering was strongly in the forward direction exhibiting a stripping type mechanism with reactions resulting from large $b$ collisions. With increasing $J$ in the HCl ($v = 1$, $J$) products, the scattering begins to exhibit an additional component in the backward direction. Lower rotational excitation in the forward scattered products is consistent with the relatively weak interaction experienced in a large $b$ stripping reaction where the $CH_3$ acts as a spectator. The backward scattered products have a slight

increase in rotational excitation due to more effective momentum coupling in a smaller $b$ collisions, providing an additional torque on the departing HCl product.

### 3.3 Cl + Ethane

The reaction of Cl with ethane is slightly endothermic by ca. 2 kcal/mol. It was found[14] that only a small fraction (2%) of the available energy was partitioned into the HCl product rotation. It was also determined that there was very little internal excitation in the ethyl radical product. While these results were consistent with a developing picture of direct collinear H-atom abstraction, the nearly isotropic angular distribution was a remarkable departure from the case of methane. This difference was explained as the result of the much lower reaction barrier in the $C_2H_6$ reaction. To overcome the substantially lower barrier to reaction, only a little of the total translational energy is required along the reaction coordinate. Therefore, in contrast to the strict restriction of $b$ for the reaction with methane, a larger range of $b$ leads to reaction, resulting in the nearly isotropic angular distribution. The ethyl radical products have also been detected, and the results obtained by detection of the two products respectively agreed with each other very well.

### 3.4 Cl + Propane/Isobutane

Using the same technique, Varley and Dagdigian have extended their studies to include larger hydrocarbons, propane and isobutane.[15–17] The collision energies were 7.4 kcal/mol and 8.1 kcal/mol respectively. Competing with the primary H atom abstraction, there are secondary H atom abstraction for propane and tertiary H atom abstraction for isobutane. Abstractions of all three types of H atoms are exothermic, with the exothermicity increasing through the order of primary, secondary, and tertiary. Using isotopically labeled reactants the authors were able to separate abstraction of different H atoms. Both secondary and tertiary H atoms were abstracted preferentially as compared with the neighboring primary H atoms. This result was also noted previously for propane by Yen *et al.*[21] The HCl/DCl products were found to be rotationally cold, which was in agreement with previous studies of smaller hydrocarbons, again implying a linear Cl–H–C intermediate geometry. However, the rotational excitation of the HCl/DCl products from secondary and tertiary H atoms abstraction was found to be

slightly higher than that of primary H-atom abstraction. Abstraction of the primary H-atoms in both molecules showed mostly backward scattering, and secondary and tertiary H-atoms abstraction showed more isotropic and sideways scattering, respectively. The greater reactivity, slightly higher rotational excitation, and more isotropic scattering reflect that a larger range of b leads to the reaction, which is consistent with the very low activation barriers reported for both reactions from kinetic studies.[4]

## 3.5 Cl + Propane/Pentane: Crossed Molecular Beam Investigation

Suits and coworkers have investigated the dynamics of reactions of Cl with propane[18] and pentane[19] using the well established crossed molecular beam machine using VUV synchrotron radiation to probe the alkyl radical product. Compared with the "universal" electron impact ionization method, VUV synchrotron radiation ionization has the advantage that there is no background generated from dissociative ionization of scattered alkane reactant if the photon energy of the VUV light is tuned to above the ionization potential (IP) for the alkyl radical but below the IP for the alkane. They measured the laboratory frame TOF spectra at various angles, from which the CM frame flux maps were generated. The continuous atomic chlorine beam was generated by thermal dissociation of $Cl_2$ diluted in rare gas mixtures at 1500–1550°C. At 1500°C a Boltzmann distribution predicts that ca. 15% of the chlorine atoms will be in the excited spin-orbit state ($^2P_{1/2}$). It was believed that a large percentage of these excited Cl was relaxed in the supersonic expansion and that the majority of the Cl reactants should be in the ground spin-orbit state ($^2P_{3/2}$).

The reaction of Cl with propane was investigated at three collision energies, $E_c$ = 8.0, 11.5, 31.6 kcal/mol. The measurements showed very broad scattering at all three collision energies. The translational energy release for forward scattered products was greater than sideways/backward scattered products. This dependence of the translational energy release on the scattering direction was most apparent at the two higher collision energies. Furthermore, the translational energy release in the forward scattered products appeared to scale with the collision energy. This was explained by contributions from two distinct reaction mechanisms. The forward scattering component was from a stripping reaction with large impact parameters; the sideways/backward scattering component was from direct collinear abstraction with small impact parameters.

The reaction of Cl with pentane was investigated at collision energy 16.8 kcal/mol. Again, two components of scattering were observed. For the forward scattering component, the translational energy release peaked at the maximum energy available for forming secondary pentyl radicals, with an average of only 1.8 kcal/mol remaining in internal degrees of freedom; this component was attributed to a stripping mechanism. For the backward/sideways scattering component, the translational energy release peaked at 6.8 kcal/mol while the average being 7.7 kcal/mol, counting for only 35% of total available energy; this immediately meant that the internal energy of the pentyl radical was significant because previous studies showed that the internal energy of the HCl product was very low. The authors argued that the high internal energy in pentyl radical product might indicate the participation of the extended carbon backbone in the reaction. However, the "vertical H-atom transition" mechanism we proposed for the O + alkane reaction (discussed in Sec. 5) may give a more reasonable explanation. Calculations showed a collinear transition state geometry for these reactions, and the authors argued this could be reconciled with the forward scattering if the transition state were not tight.

However, these results of Cl + propane/pentane reactions are far from fully understood. Ahmed and coworkers have examined these reactions[22] using the experimental approach similar to that used for Cl + ROH reactions (Sec. 4). They found similar results for the backward/sideways scattering component, but observed little or none of the forward scattering component. They also did not observe the forward component in any of the Cl + ROH reactions. The source of this significant discrepancy is still an open question. A possible reconciliation of the difference between the two studies may lie in the source of Cl atoms used in the two sets of experiments. Ahmed *et al.* use a photolytic source and have carefully characterized the Cl beam to be of predominantly ground state character. In the Cl-hydrocarbon experiments, the Cl atom beam was generated by thermal dissociation of $Cl_2$ in a heated nozzle maintained at 1500–1550°C, and a Boltzmann distribution as stated by the authors predicts that ca. 15% of the chlorine atoms will be formed in spin-orbit excited state, Cl ($^2P_{1/2}$). While the excited state component of the Cl beam was not explicitly determined, the authors assumed that the supersonic expansion would relax the spin-orbit excited component of the beam. Traditional wisdom has it that the spin-orbit excited atoms are less reactive; however, recently Liu and coworkers have seen enhanced reactivity with spin-orbit excited Cl[23] and F[24] atoms, respectively. They find the spin-orbit excited atoms show very

different dynamical behavior compared to their ground state counterparts. To account for the forward scattering, the Cl* would have to be much more reactive. In any case, it would be very interesting to study the effect of spin-orbit excitation of the Cl atom on its reaction dynamics with alcohols and hydrocarbons. Another possible explanation for the difference in the experiments concerns the nature of the probe. The imaging studies rely on single photon ionization at 157 nm, and this will not detect primary hydrocarbon radicals very efficiently, if at all. The synchrotron studies, on the other hand, relied on photoionization at much higher energies so that the relative detection efficiency for primary vs. secondary radical detection may be quite similar. If the forward scattering is associated with primary H abstraction, then this discrepancy between the two experiments could be explained. However, the thermodynamics and the translational energy release appeared to rule out forward scattering for the primary radicals, certainly for the pentane case, so this explanation is not satisfying, either. A final possible explanation is that the forward scattering in the synchrotron studies represents inelastic scattering that is somehow detected at the radical mass. At this time, a convincing explanation for these discrepancies is not forthcoming.

## 4 H Atom Abstraction Reactions Cl + ROH → HCl + Hydroxyalkyl Radical

### 4.1 *Introduction*

While there have been a number of detailed dynamical studies performed on H abstractions from saturated hydrocarbons, analogous studies of H abstraction from alcohols are very rare, despite the fact that alcohol oxidation has broad practical significance. With the advent of improved $F_2$ excimer laser technology and the development of the velocity map imaging technique, Suits and coworkers have undertaken a series of experiments to study the dynamics of H abstraction reaction of ground state Cl ($^2P_{3/2}$) atoms with alcohols ($CH_3OH$, $C_2H_5OH$ and 2-$C_3H_7OH$).[25,26] The corresponding hydroxyalkyl radical was detected via single photon ionization using 157 nm laser light. The double differential cross sections were obtained at collision energies of 8.7 kcal/mol for methanol, 6.0 and 9.7 kcal/mol for ethanol, and 11.9 kcal/mol for 2-propanol.

## 4.2 *Experimental and Image Analysis*

The crossed molecular beams apparatus has been described in detail in previous publications from the group.[27,28] Figure 1 shows the schematic. The Cl beam was generated by 193 nm photodissociation of oxalyl chloride [$(ClCO)_2$] seeded in He at the nozzle of a Proch–Trickl piezoelectric pulsed valve. The photodissociation of oxalyl chloride at 193 nm yields predominantly Cl, Cl* and CO. The Cl/Cl* atom beam velocity and spread was monitored using (2 + 1) REMPI technique, and the Cl*/Cl ratio was obtained to be 1 : 50 and 1 : 62 for oxalyl chloride seeded in He and Ar respectively. It is believed that efficient quenching of Cl* happens due to many Cl–CO collisions. The speed ratio ($v/\Delta v$, FWHM) for the Cl beam was 5.8 (in He) and 2.3 (in Ar), respectively. The alcohol (methanol, ethanol, 2-propanol) seeded 2% in He was expanded through another Proch–Trickl pulsed valve, collimated by a single skimmer and the beams were allowed to interact on the axis of the velocity focusing time-of-flight mass spectrometer. For the ethanol experiments, the collision energy was reduced by seeding the oxalyl chloride in Ar. The speed ratio for the alcohol beams was greater than 12 in all cases.

Light from a 157 nm excimer laser (1–2 mJ, 10 Hz) was focussed loosely into the interaction region of the two crossed beams and used to ionize the hydroxyalkyl radical reaction product. The velocity of the ions was measured by using velocity map imaging technique, with a 80-mm diameter

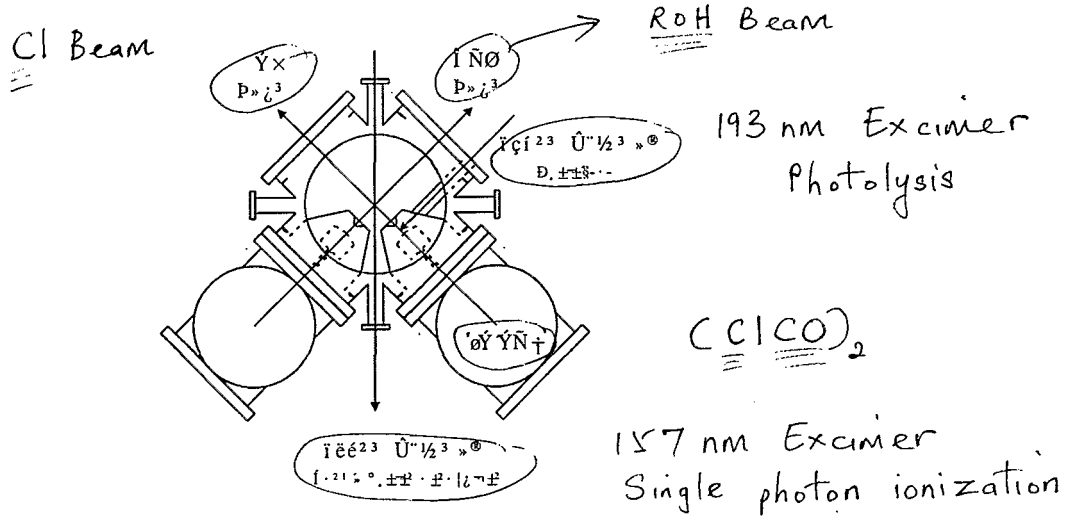


**Fig. 1.** Experimental schematic for crossed beam studies of Cl + alcohol reactions.

dual microchannel plate (MCP) detector coupled to a fast phosphor screen (P-47), which was viewed by a fast-scan charge-coupled-device camera with integrating video recorder. The ion yields were far below levels at which space charge effects would play a role. Camera threshold and gain were adjusted in conjunction with a binary video look-up table to perform integration of single ion hits on the MCP free of video noise. The recorded image, which is actually a 2D projection of the nascent 3D velocity distribution, was analyzed by established tomographic techniques to reconstruct the 3D distribution.

There was substantial hydoxyalkyl product from photodissociation of the alcohol reagent at 157 nm, which showed up as a small ring centered at the alcohol beam and created a problem in extracting information for the most sharply forward-scattered products relative to the incoming alcohol beam. While analyzing the images, the authors omitted the region involved with the photochemistry background since subtractions of background did not yield reliable results in the region (e.g. see Fig. 3(a)). Fortunately, this was limited to the most sharply forward portion of the distributions, where the fraction of the product flux appears to be small. Efforts were made to minimize the complications associated with crossed-beam experiments, so that they can use direct inverse Abel transform to reconstruct the 3D image. These efforts include: (1) employing intense, sharp pulses using piezo valves and a photolytic Cl atom source, so that the arrival of the Cl beam pulse was very abrupt; (2) probing immediately after the arrival of the Cl beam pulse, even though the signal there was not a maximum, so that reactions occurring prior to the probe laser contributed little to the image; and (3) using a large probe volume relative to the beam interaction volume, which was made practical by their single photon probe method. Monte Carlo simulations of the detection efficiency as a function of the recoil velocity[27] justified their using of the inverse Abel transform method to reconstruct the full 3D distributions.

## 4.3 *VUV Single Photon Soft Ionization as a "Universal" Approach: Dependence on the Target Internal Energy?*

VUV photoionization is emerging as a valuable alternative to electron impact ionization as a soft, universal probe of reaction products. This has been stimulated by the development of intense VUV sources such as the Chemical Dynamics Beamline at the Advanced Light Source,[29,30] and by the development of stable, reliable $F_2$ excimer lasers. The Davis group

at Cornell has used $F_2$ excimer lasers in crossed-beam studies of transition metal reactions.[31,32] As described in this chapter, our group has used this probe extensively to detect reaction products from crossed-beam imaging experiments. The use of 157 nm single-photon ionization provides great sensitivity, but raises the question of the possibility of the probe sensitivity varying strongly with internal energy in the product. Indeed this is an important issue with any probe technique, whether it is REMPI, LIF, or electron impact-mass spectrometry. However, this issue is rarely been investigated in much detail. To explore this issue directly, we studied the photodissociation of 2-chlorobutane at 193 nm giving chlorine atom and 2-butyl radical,

$$CH_3CHClCH_2CH_3 \rightarrow Cl + CH_3\dot{C}HCH_2CH_3 \quad \Delta H_f^\circ(298\,K) = 84.9\,kcal/mol, \tag{6}$$

and compared two distinct probe approaches, REMPI probe of the chlorine atom and the 157 nm universal probe of the 2-butyl radical cofragment.

The experimental apparatus has been described in the above subsection, but for this purpose we only use one molecular beam, namely 2-chlorobutane replacing the alkane in the scattering setup. Neat vapor of 2-chlorobutane at room temperature with a pressure of about 0.2 atm was used to generate the molecular beam. The beam was photolyzed by a 193 nm ArF excimer laser (~4 mJ/pulse), and two probe approaches were used respectively to measure the translational energy release spectrum. One is to probe the chlorine atoms via REMPI[33] at ~235 nm (~2 mJ/pulse). This probing light was the doubled output of a tunable dye laser, which was pumped by the 355 nm output of a Nd:YAG laser. The other is to probe the butyl radical using 157 nm single photon ionization. In either approach, the products were detected via velocity map imaging. The CM 3D images were reconstructed using the inverse Abel transform, from which the translational energy distributions were derived. Chlorine image acquisition involved scanning over the Doppler profile and subtracting the background photochemistry generated by the probe laser. For butyl, the background produced by the 157 nm probe alone was likewise excised.

At 193 nm, the available energy from 2-chlorobutane photodissociation (Eq. 6) is 63.9 kcal/mol.[34] The relative spin-orbit state populations were obtained by integrating the total signal for Cl, obtained on the $(4p\,^2D_{3/2} \rightarrow 3p\,^2P_{3/2})$ transition at 235.336 nm and Cl* obtained on the $(4p\,^2P_{1/2} \rightarrow 3p\,^2P_{1/2})$ transition at 235.205 nm with background

subtracted as described. Using the relative linestrength 1 : 0.6 for these two transitions,[28] we obtain a value of $0.50 \pm 0.04$ for $Cl^*/(Cl+Cl^*)$.

Ion images for Cl, $Cl^*$ and butyl radical from the 193 nm dissociation of 2-chlorobutane were acquired and analyzed using the inverse Abel transform. The results are summarized in Fig. 2. Here, the total translational energy is presented as determined assuming momentum conservation with the undetected fragment, and thus the translational energy release distributions obtained for Cl and $C_4H_9$ may be compared directly. In Fig. 2(b), we compare the total translational energy distribution derived from the butyl radical detection with that determined from $Cl/Cl^*$ detection, which is a weighted average of the two distributions of Fig. 2(a) according to their measured populations. The agreement, although not perfect, is quite reasonable and no systematic deviations are apparent.

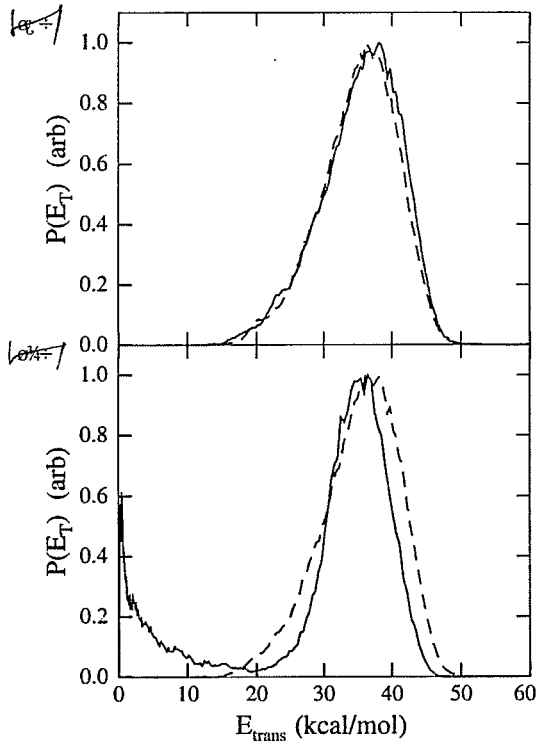


**Fig. 2.** Total translational energy release distributions from the photodissociation of 2-chlorobutane at 193 nm for (a) Cl (solid line) and $Cl^*$ (dashed line); and (b) butyl radical (solid line) and average $Cl/Cl^*$ (dashed line).

There is a strong feature at very low recoil energy for the butyl fragment, and this feature appears for most systems we have studied using the 157 nm probe. We believe it arises from dissociative ionization of chlorobutane clusters in the beam, although we have not studied it in detail. We just omit this portion of the distribution for comparison of the average translational energy release. From the data in Fig. 2(b), the average translational energy release is found to be 34.0 kcal/mol based on the Cl product, and 35.0 kcal/mol based on the butyl product. The peaks in both cases are very near the average value.

## 4.4 *Results: Cl + ROH*

### 4.4.1 *Cl + Methanol*

There are two channels for the reaction of Cl with methanol:

$$\mathrm{Cl} + \mathrm{CH_3OH} \rightarrow \mathrm{CH_3O} + \mathrm{HCl} \quad \Delta H = +2.4\,\mathrm{kcal/mol}, \tag{1}$$

$$\rightarrow \mathrm{CH_2OH} + \mathrm{HCl} \quad \Delta H = -6.8\,\mathrm{kcal/mol}, \tag{2}$$

forming the methoxy ($CH_3O$) and hydroxymethyl ($CH_2OH$) radicals respectively. The branching ratio of channel (2) has been found experimentally[35] to be close to unity, 0.95. The 157 nm probe will not be sensitive to channel (1), because the IP of $CH_3O$ (10.42 eV)[36] is higher than the single photon energy of probe laser and the $CH_3O^+$ ion is unstable.[37] Channel (2), however, can be readily probed by single photon ionization using the 157 nm laser light, because the ionization potential of $CH_2OH$ is 7.56 eV.[34]

Figure 3(a) shows an image of the product formed at mass 31, believed to be $CH_2OH^+$ (channel (2)) only, from the reaction of Cl with methanol at a collision energy of 8.7 kcal/mol. The Newton diagram is superimposed on the image. The total available energy is 15.5 kcal/mol for the measured channel. The outer ring in Fig. 3(a) shows the maximum recoil speed allowed for the $CH_2OH$ radical; there is reactive flux virtually to the limit of available energy in the sideways and backward direction. The CM angular distributions, extracted from the images are shown in Fig. 3(b). There is substantial sideways scattering—the integrated ratio of sideways (45–135°) to backward (135–180°) is 1.75. Figure 3(c) shows the translation energy distribution obtained from the reconstructed data. The maximum available energy is indicated in the figure. The average translational energy released is 6.1 kcal/mol, 39% of the available energy.

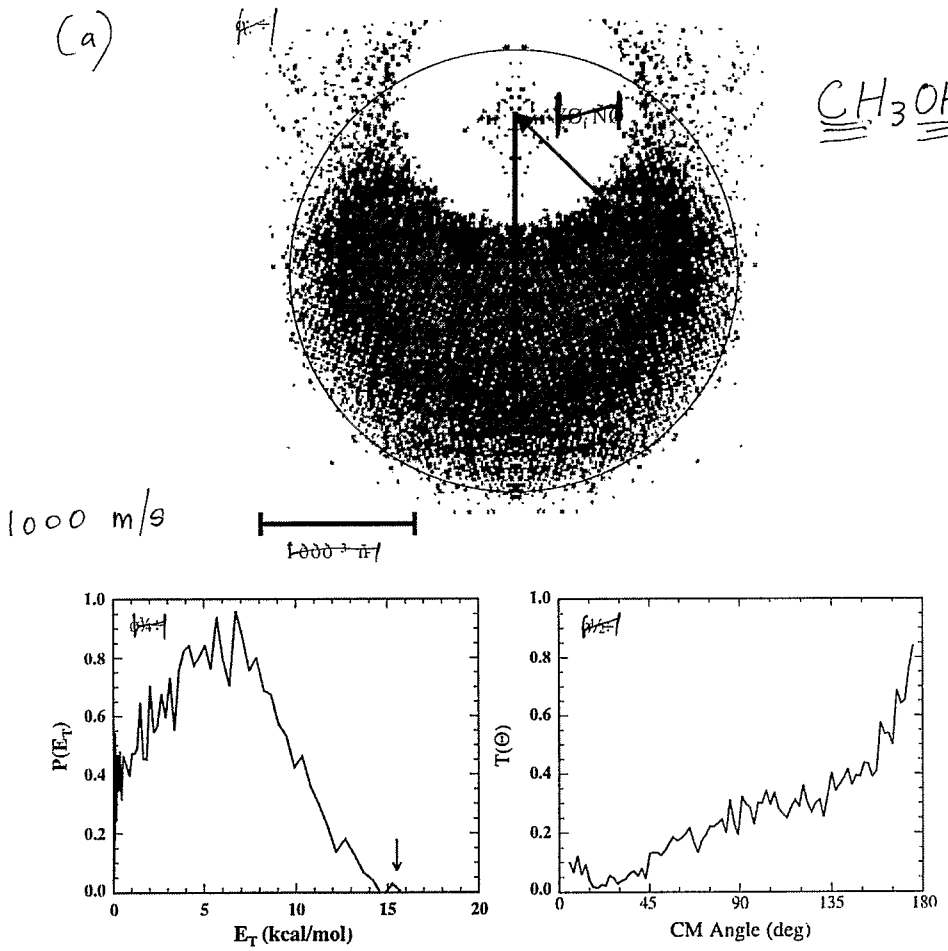


**Fig. 3.** Cl + $CH_3OH$ reaction at 8.7 kcal/mol collision energy. (a) Raw image of $CH_2OH$ product probed by 157 nm single photon ionization. Superimposed are the Newton Diagram and a ring representing the speed limit. (b) Total translational energy distribution obtained from reconstructed image. The arrow shows the total available energy. (c) Angular distribution obtained from reconstructed image.

4.4.2 Cl + Ethanol

The abstraction of an H atom from ethanol by the Cl atom can give rise to three different radicals as shown below:

$$C_2H_5OH + Cl \rightarrow CH_3CHOH + HCl \quad \Delta H = -9.3\,\text{kcal/mol}, \quad (3)$$

$$\rightarrow CH_2CH_2OH + HCl \quad \Delta H = 0.5\,\text{kcal/mol}, \quad (4)$$

$$\rightarrow CH_3CH_2O + HCl \quad \Delta H = 4.5\,\text{kcal/mol}. \quad (5)$$

Unambiguously, the 1-hydroxyethyl radical ($CH_3CHOH$) channel can be readily probed and the ethoxy radical ($CH_3CH_2O$) channel cannot, for their IPs (6.64 eV,[38] 10.29 eV[39]) are far below and far above the single photon energy (7.86 eV) of the 157 nm probe laser, respectively. However, it is not so clear with the 2-hydroxyethyl radical ($CH_2CH_2OH$), since the IP for 2-hydroxyethyl is by no means conclusive. Ruscic and Berkowitz[39] quote a figure of $8.18 \pm 0.08$ eV, but they infer an I.E. of $\sim$7.7 eV depending on the thermodynamic cycle and bond dissociation energies employed in generating the result. A G-2 theoretical result[40] posits 7.58 eV as the adiabatic ionization energy for the 2-hydroxyethyl radical. Khatoon *et al.*[41] carried out an end product analysis experiment to measure the rates of this reaction and also derive the branching ratio for the formation of the three different radicals. They conclude, for the reaction of Cl with alcohols, that no abstraction from the OH group was observed and that the abstraction from the alkyl groups followed the thermodynamically favoured route by forming mainly secondary radicals. Based on these considerations, Ahmed and coworkers suggested that the mass 45 detected was the 1-hydroxyethyl radical only.

Reactive scattering experiments with ethanol were performed at two collision energies $E_{coll}$ =6.0 kcal/mol and 9.7 kcal/mol, and the raw images are shown in Fig. 4(a) and 4(b) respectively. At 6.0 kcal/mol, the reactive flux is predominantly in the backward hemisphere. When the collision energy is increased to 9.7 kcal/mol, there is enhanced sideways scattering, and the raw image begins to resemble the methanol system. However, for ethanol at both collision energies the reactive flux does not extend out to the thermodynamic limit. The average translational energy release is 38% and 32% of the available energy for $E_{coll}$ =6.0 kcal/mol and 9.7 kcal/mol, respectively. The translational energy distributions obtained from the reconstructed data are shown in the upper panel in Fig. 4(c). The corresponding angular distributions are shown in Fig. 4(d), normalized to the same maximum in the backward direction. As is apparent in the raw images, there is a significant enhancement in sideways scattering with an increase in collision energy. There is also substantial coupling between translational energy release and corresponding angular distributions. Fig. 4(e) compares the translational energy release for the sideways (50–130°) to backward (130–180°) components at a collision energy of 6.0 kcal/mol. The average energy release for the sideways scattering is 4.7 kcal/mol; the backward scattering is faster, with an average of 6.6 kcal/mol translational energy.

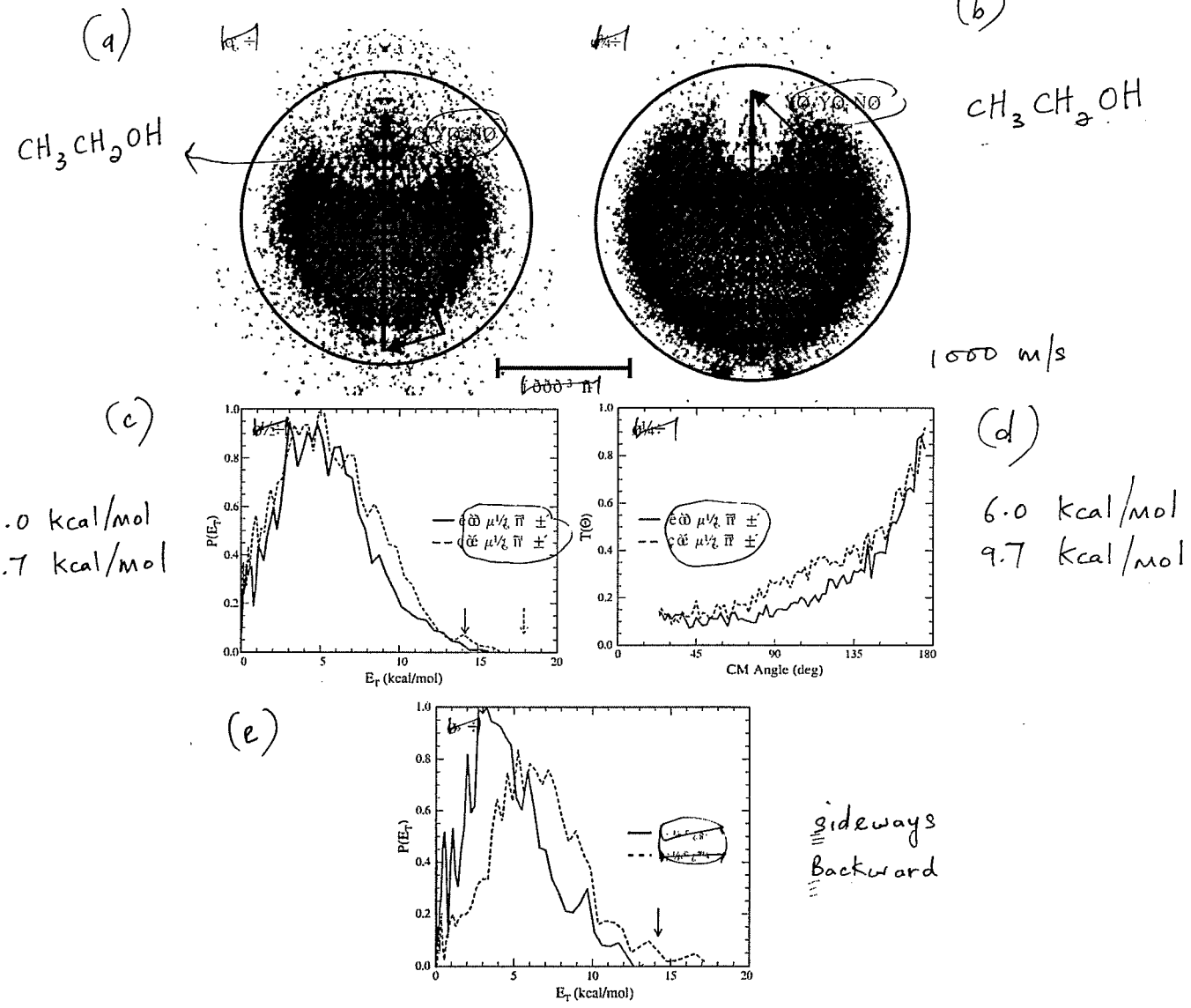


**Fig. 4.** Cl + $CH_3CH_2OH$ reaction. (a) and (b): Raw image of mass 45 ($CH_3CHOH$) at collision energy of 6.0 and 9.7 kcal/mol respectively. Superimposed are the Newton Diagram and a ring representing the speed limit. (c) Total translational energy distribution obtained from reconstructed images. The arrow shows the total available energy. (d) Angular distribution obtained from reconstructed image. (e) Comparison of the translational energy distributions in the backward scattering and sideways scattering at collision energy 6.0 kcal/mol.

### 4.4.3 *Cl + Isopropanol*

There are several channels for the H atom abstraction of Cl from isopropanol, producing different radicals. The ionization energies for the possible product radicals are not available, except for 9.2 eV for the 1-Methyl ethoxy radical,[42] the product of hydroxyl H abstraction. However, analogy to the systems above suggests a much lower IP for the $(CH_3)_2COH$ radical, and Ahmed and coworkers suggested this to be the most likely candidate for their detected product at mass 59 in this reaction. An image recorded at mass 59, corresponding to $(CH_3)_2COH^+$, at 11.9 kcal/mol collision energy is shown in Fig. 5(a). The scattering is predominantly in the backward hemisphere and the image resembles the ethanol case with low collision energy. Figures 5(b) and 5(c) show the translational energy release and angular distributions. Again it is shown that the energy release is not to the thermodynamic limit.

Table 1 summarizes the results for all the alcohols studied by Ahmed and coworkers. All the translational energy distributions peak around 6 kcal/mol, irrespective of the alcohol reagent and collision energy. Another common thread is that the fraction of energy going into translation is similar for all the alcohols.

## 4.5 *Discussion: Cl + ROH*

The reaction of methanol with chlorine atoms has been studied in a number of laboratories using traditional kinetic methods[43] and the consensus is that the hydroxymethyl radical formation channel is predominant. The rate of reaction is moderately fast, $(5.3\text{–}6.3) \times 10^{-11}\,cm^3\,molecule^{-1}\,s^{-1}$, with no appreciable barrier. However, experimental studies on the dynamics of H abstraction from methanol are rare.

Jodkowski *et al.*[43] have performed *ab initio* calculations at different levels of theory and using several basis sets to characterize stationary points on the potential surface for the reaction of Cl with $CH_3OH$. They found several minima, including one in the entrance channel corresponding to Cl attaching to the O atom and another in the exit channel resembling a hydrogen bonded complex between HCl and $CH_2OH$. The latter represents the minimum point on the surface, 10.0 kcal/mol below the reactants. The presence of these minima led them to suggest that reaction occurs via formation of an intermediate complex similar to the $CH_3OH$ + F reaction.[44] No exit-barrier was found in their calculation for the $CH_2OH$ + HCl channel.

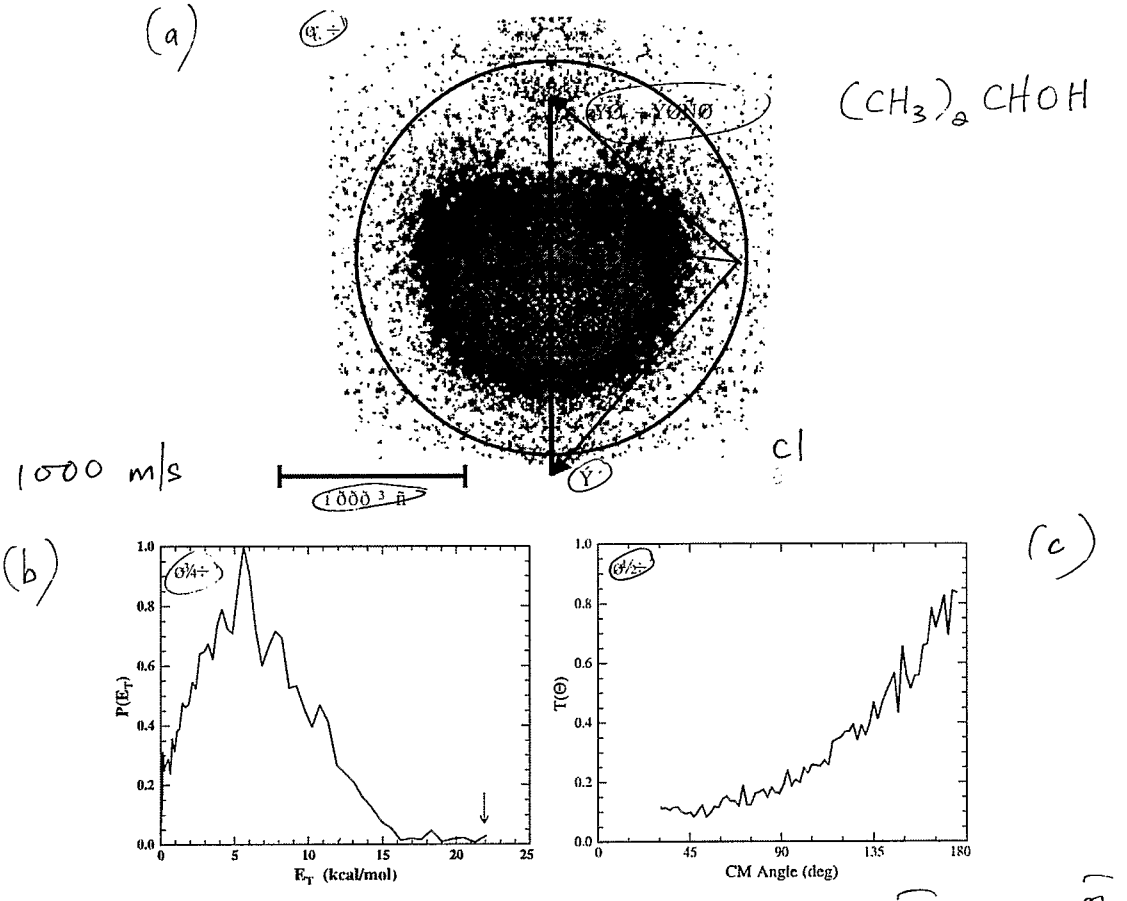


**Fig. 5.** Cl + $(CH_3)_2CHOH$ reaction. (a) Raw image of mass 59, $(CH_3)_2COH^+$, at collision energy of 11.9 kcal/mol. Superimposed are the Newton Diagram and a ring representing the speed limit. (b) Total translational energy distribution obtained from reconstructed image. The arrow showing the total available energy. (c) Angular distribution obtained from reconstructed image.

However, they generated only a few stationary points on the surface and did not explicitly consider the reaction path.

According to the above results from Ahmed and coworkers' study, however, there clearly exists a direct reaction mechanism, at least at 8.7 kcal/mol collision energy, because the products are exclusively sideways-backscattered. Although there is background problem in the sharply forward-scattered region, in all cases they can rule out the forward-backward symmetry characteristic of collision complexes. All of the

Table 1. Summary of translational energy distributions. $E_{coll}$: Collision energy; $E_{avl}$: Total energy available; $\langle E_{tr} \rangle$: Average translational energy release; $f_{tr}$: fraction of total energy appearing in translation; $R_{side/back}$: Ratio of side-scattered to backscattered flux (see text).

| ROH | $\langle E_{coll} \rangle$ (kcal/mol) | $E_{avl}$ (kcal/mol) | $\langle E_{tr} \rangle$ (kcal/mol) | $f_{tr}$ | $R_{side/back}$ |
|---|---|---|---|---|---|
| $CH_3OH$ | 8.7 | 15.5 | 6.1 | 0.39 | 1.75 |
| $C_2H_5OH$ | 6.0 | 14.2 | 5.4 | 0.38 | 1.23 |
| $C_2H_5OH$ | 9.7 | 17.9 | 5.7 | 0.32 | 1.64 |
| $C_3H_7OH$ | 11.9 | 21.9 | 6.8 | 0.31 | 1.33 |

observed angular distributions can be interpreted as results of implying direct, close (small but nonvanishing impact parameter) collisions.

Khatoon *et al.*[41] have studied the kinetics and mechanism of reaction of Cl with ethanol ($1.2 \times 10^{-10}\,cm^3\,molecule^{-1}\,s^{-1}$) and 1- and 2-propanol. For the reaction of Cl atoms with alcohols, no abstraction from the OH group was observed, and abstraction from the alkyl groups followed the thermodynamically favored route by forming mainly secondary radicals. J. Edelbuttel-Einhaus *et al.* reported a rate constant of $7.84 \times 10^{-11}\,cm^3\,molecule^{-1}\,s^{-1}$, and obtained a branching ratio of 1 : 20 between reactions 4 and 3, confirming that the 1-hydroxyethyl radical is predominantly formed.

The scattering studies shown in this section have demonstrated the effect of collision energy. At low collision energy, scattering is predominantly in the backward hemisphere. With an increase in collision energy the scattering is enhanced in the sideways direction with no concomitant increase in the translational energy release. The angular distributions for ethanol at the higher collision energy begins to resemble that of methanol, suggesting that larger impact parameter collisions begin to play a role, or deviations from collinearity may be more important. The translational energy release is reduced in the sideways direction, implying greater internal energy in the larger impact parameter collisions. This is consistent with greater rotational excitation for these sideways scattered products.

The energies of the C–H bonds in ethanol and propane are very similar; furthermore, the structures resemble each other. So, it is interesting to compare the results for Cl–$C_2H_5OH$ with Cl–$C_3H_8$. Ahmed and coworkers do not observe the large impact parameter-dominated fast forward-sideways scattering reported in the case of propane by Blank *et al.*[18] However, for

the low impact parameter sideways-backward scattering there is qualitative agreement between these two studies. Blank *et al.* saw strong coupling between their angular and translational energy distributions, again this is in agreement with the above results for Cl–$C_2H_5OH$. Blank *et al.* found a much larger fraction of available energy in translation than in the Cl-ethanol reaction, and this fraction changed little with collision energy ($\langle E_T \rangle / E_{avail}$ = 0.53, 0.52, 0.48 for $E_{coll}$ = 8.0, 11.5, 31.6 kcal/mol). An examination of column 5 in Table 1 shows qualitatively similar behavior for $C_2H_5OH$.

Following in a similar vein, scattering for the Cl–$C_3H_7OH$ system should resemble the Cl–$C_5H_{12}$ system. In the case of the Cl-isopropanol system, the angular distributions are qualitatively quite similar to the backward scattering (channel 2) reported in the Cl–$C_5H_{12}$ system.[19] Hemmi and Suits[19] saw a broad backward scattering distribution with about 35% of the available energy being deposited into product translation, similar to the 31% here in the Cl–$C_3H_7OH$ system. And just as in the propane case, Hemmi and Suits observed a distinct forward-sideways scattered component with almost all the available energy being deposited into product translation. Hemmi and Suits invoked the participation of the carbon skeleton in the scattering process to account for the substantial internal energy deposited in the hydrocarbon radical fragment. However, with the conclusions of our recent studies of O + alkane reactions, it seems reasonable to suggest that the "vertical" reaction mechanism may also apply to the H atom abstraction by Cl atom (see Sec. 5 below).

Given the similarity in the sideways-backward scattering between the Cl-alcohol and Cl-hydrocarbon systems, Ahmed and coworkers, however, do not observe the analogous fast forward-sideways scattering component seen by Suits and coworkers in their Cl-hydrocarbon experiments. Actually, as discussed in Sec. 3.5, Ahmed *et al.* have also studied the Cl + HR reactions using the same experimental setup as for this Cl + ROH study, but they did not observe the forward-sideways scattering component either.[22]

## 5 Reactions O($^3P$) + Alkanes → OH ($^2\Pi$) + Alkyl Radicals

### 5.1 *Introduction*

The reactions of ground state oxygen atoms with saturated hydrocarbons represent a cornerstone in our understanding of polyatomic reaction dynamics. Very recently, using ion imaging technique and VUV single photon

ionization probe of the alkyl radical product, our group reported the first investigation of the global dynamics of these reactions,[45,46] affording new insights into this classic problem. Prior to this study, essentially all experimental studies of the dynamics of these reactions had relied upon probing of the OH product during the previous two decades of investigation, and detailed translational energy and angular distributions had never been obtained.[47] This new imaging study is presented in this section, after a brief review of previous studies.

The major product channel of the reactions of ground state oxygen atoms with saturated hydrocarbons is to produce OH($^2\Pi$) and the alkyl radical,[48,49] and these reactions are often used as model systems for understanding H abstraction dynamics. Moreover, these reactions play an important role in combustion and atmospheric chemistry. There have been extensive investigations of the dynamics, and distinct hydrocarbon reagents have been used to study the different dynamics of reaction with primary, secondary or tertiary hydrogen atoms. This effort has recently been summarized in a lucid review by Ausfelder and McKendrick.[47] There have also been very extensive experimental kinetics studies[1–3] on these reactions, and they have established the presence of a significant barrier to reaction and provided evidence for a marked steric hindrance for the reactions. The barrier heights[3] are reported to be about 8.1, 5.3, and 5.0 kcal/mol for reaction with primary, secondary, and tertiary hydrogen atoms respectively, whereas these experimentally estimated values vary by about 1.2 kcal/mol. The corresponding reaction enthalpies at 298 K are −1.9, −6.7, and −8.9 kcal/mol, respectively.[47]

Andresen and Luntz conducted the first dynamics studies[50,51] of these reactions in 1980, in which they measured the internal state distribution of OH product via laser-induced fluorescence, with an effusive O atom source and under crossed beam conditions. In addition, they reported theoretical quasiclassical trajectory (QCT) calculations on a model potential surface. They investigated O($^3P$) reactions with neopentane, cyclohexane, and isobutane, representing primary, secondary, and tertiary hydrogen atom reaction, respectively. The OH products were found to be rotationally cold, regardless of the nature of the hydrocarbon reagent. The OH vibrational excitation, on the other hand, was found to be very sensitive to the nature of the carbon site from which the hydrogen was abstracted, increasing markedly through the order from primary, secondary, to tertiary H atom target. At 7.1 kcal/mol collision energy, they found the ratio $\sigma(v = 1)/\sigma(v = 0)$ to be 0.01, 0.24, and 1.4, for primary, secondary and

tertiary H atoms, respectively. They identified a collinear H atom abstraction mechanism, and this conclusion was supported by their trajectory calculations on a model triatomic London–Eyring–Polanyi–Sato (LEPS) potential surface intended to simulate reaction with a secondary H atom. Also using LIF detection of the OH product but employing a supersonic $O(^3P)$ beam source, Whitehead and coworkers[52,53] obtained better definition of the collision energy and considerably expanded the range of target molecules. More recently, McKendrick and coworkers[47,54] extended the studies to include the first two members of saturated hydrocarbon family, methane and ethane, and in particular they have used the OH spin-orbit state distribution, long known to be non-statistical, as a probe of nonadiabatic dynamics in this system.

Using polarized Doppler spectroscopy under bulb conditions, Kajimoto and coworkers[55] recently studied the dynamics of these reactions. They reported results for the OH $v = 1$ product from reaction of $O(^3P)$ with cyclohexane and isobutane. They obtained the first experimental differential cross sections for these reactions, although only for the vibrationally excited OH product and with a broad spread of collision energy. They inferred significant internal excitation in the alkyl radical as well. At low collision energy, they found a backscattered angular distribution as was predicted in the original theoretical studies by Luntz and Andresen. However, with increased collision energy, they found that the forward scattering becomes comparable to the backward scattering, and proposed the onset of the stripping pathway to account for this, a marked departure from previous work.

One earlier study directly probed the internal energy in the alkyl fragment, in the case of $O(^3P)$ reaction with methane.[56] While the study was focused primarily on $O(^1D)$ reaction, results for $O(^3P)$ were also reported for comparison. Their approach consisted of $SO_2$ photolysis as the O atom source, with cw diode laser probe of the methyl product under bulb conditions at relatively high pressure. Although the long time scale and high pressure precluded rotational resolution, their results showed substantial umbrella-mode excitation.

While the experimental studies explored quite a few systems, most of the *ab initio* studies of these and related reactions are actually limited to $O(^3P)$ + methane. The earliest studies simply tried to determine the transition state geometry and the height of the barrier.[57] Simply based on correlation arguments, the $^3E$ surface, for which one of the O atom unpaired orbitals points toward the hydrocarbon, is found to be reactive, while the

$^3A_2$ surface is unreactive. The transition state was found to have a collinear geometry and this has been confirmed in many subsequent calculations. The readers are referred to the review by Ausfelder and McKendrick and references therein for more details on the theoretical studies.

In this section, we present our recent study of the dynamics of $O(^3P)$ reaction with secondary and tertiary hydrocarbons at a range of collision energies. With the apparatus adapted to provide intense $O(^3P)$ beams with easily tunable velocities, we obtained the first measurement of the differential cross-sections at well-defined collision energy. Based on these measurements, and using the OH internal energy distribution of Andresen and Luntz,[50] we also obtained the internal energy distribution of the alkyl radical product. On the basis of these results, and supporting theoretical calculations, we proposed a modification of the traditional triatomic picture used to understand the dynamics of these reactions.

## 5.2 *Experimental and Image Analysis*

The crossed molecular beam imaging machine used in the present work has been described in detail elsewhere,[28] and the detection method is similar to that described in Sec. 4. However, additional major modifications were made for purpose of the present experiment. Figure 6 shows the schematic of the setup. Two molecular beams, the alkane reactant and sulfur dioxide, are generated using piezoelectric pulsed valves. The beams are parallel with each other and 57 mm apart, with the alkane beam propagating along the axis of the ion optics toward the imaging detector. $O(^3P)$ is produced by $SO_2$ photolysis at 193 nm. The 193 nm laser (~100 mJ/pulse) crosses the $SO_2$ precursor beam upstream from the 157 nm laser (~1 mJ/pulse) probe spot, with a distance adjusted with the desired collision energy so that the nominal relative velocity of the reagents is parallel with the surface of the detector. The main advantage of this configuration is that the longitudinal spread in the molecular beam velocities is perpendicular to the relative velocity vector, so that only the transverse spread contributes significantly. The alkyl products are detected using velocity map imaging[58,59] with 157 nm single photon ionization. We do not consider primary H abstraction mainly owing to the fact that the IP of the product radicals are out of reach with our 7.86 eV probe. In addition, the barriers for this process are significantly higher, so that even in cases such as *n*-butane or isobutane, where primary H atom sites are also present in addition to the secondary or tertiary sites, we need only consider the latter.

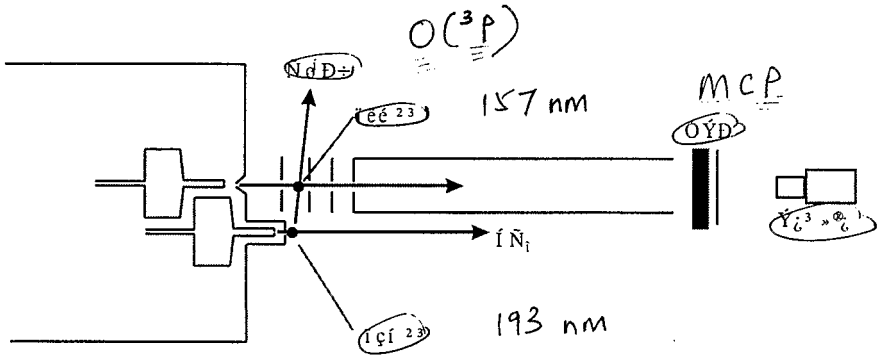


**Fig. 6.** Schematic experimental setup for the $O(^3P)$ + alkane reactions.

Photolysis of $SO_2$ at 193 nm generates fast $O(^3P)$ atoms with a range of recoil velocities and no $O(^1D)$ atoms.[60,61] By choosing the delay between the photolysis and probe laser pulses, continuously tunable $O(^3P)$ velocities are obtained. Although faster $O(^3P)$ atoms that have arrived at the alkane beam earlier may also contribute to the recorded image and in consequence broaden the collision energy spread and distort the image, it is clear from our studies, and from modeling the experiment, that the motion of the center of mass of earlier collisions rapidly carries the products away from the probe region, so that only contributions from collisions during or very near to the time of the probe pulse are important. The result is that the distortion is quite modest, and can readily be modeled and understood, and that the broadening of the collision energy is small. As a result, a broad photolysis source gives rise to a collision energy that is well-defined and easily tunable under crossed-beam conditions. Collision energies from 4 up to 15 kcal/mol are practical for the reaction with cyclohexane in our experimental setup.

Pure $SO_2$ with a backing pressure of 2.0 atm is used to generate the $SO_2$ molecular beam. For the alkane beam, pure alkane vapor is used, and the backing pressure ranges from 0.15 to 0.5 atm. It is necessary to keep the alkane beam as slow as possible to minimize the horizontal offset between photolysis and probe lasers, but a tradeoff exists between considerations of the offset and the distortion of the images from pre-probe events. When the alkyl product of the reaction is probed by the 157 nm laser, the parent alkane also produces alkyl radicals via 157 nm photodissociation. This background photochemistry, confined to the forward scattering region, does not depend on the oxygen atom beam and is subtracted by offsetting the $SO_2$ molecular beam pulse temporally so that it is missed by the 193 nm

photolysis laser. This allows for reliable, albeit noisy, data to be obtained even for the forward scattered product. However, this photochemical background does represent one of the most challenging aspects of this approach.

When the ion imaging technique is applied to the scattering studies, some inherent factors make the analysis of obtained images complicated. These factors include the finite duration of the molecular beam pulses, the spreads in the beam velocities and the size of the probe volume relative to the interaction volume. Usually one cannot simply use the straightforward transform as commonly used for photochemistry studies. These issues have been studied in detail beginning with the first such scattering experiments in the Houston group,[62,63] and a variety of computer programs have been developed in a number of groups around the world to deconvolute these instrument functions and isolate the underlying distributions.[64,65] In our present study, some particular features make an understanding of the relation between the center of mass distributions and the experimental image a crucial issue. Most significantly, we rely on a free photolytic source for the $O(^3P)$ reagent, and its inherent velocity distribution is extremely broad; indeed we tune through this distribution experimentally to adjust the collision energy. Furthermore, in the present configuration the faster oxygen atoms can interact with the alkane beam anywhere along its path; if the scattering event then puts the product alkyl radical into the probe laser volume at the time the laser fires, then detection of that product is possible. To account for all of these issues rigorously, we have adapted the original Monte Carlo program used to simulate the Ar–NO scattering studies in the Houston group[63] to our current configuration. We first note, however, the chief reason this approach works as well as it does given the limitations noted above: it is the rapid motion of the center of mass of the system away from the detection region that makes the scattering from earlier events less important than one might suspect.

All final experimental distributions were obtained by forward convolution simulations starting from the inverse Abel transformed data. It turned out that the translational energy distributions required little adjustment, but the angular distributions required some modification to fit the experimental images.

## 5.3 *Results and Discussion: $O(^3P)$ + RH*

Images of cyclohexyl radical from reactions of $O(^3P)$ with cyclohexane at 4.7, 6.6, 11.3 and 14.8 kcal/mol collision energies are shown in the left

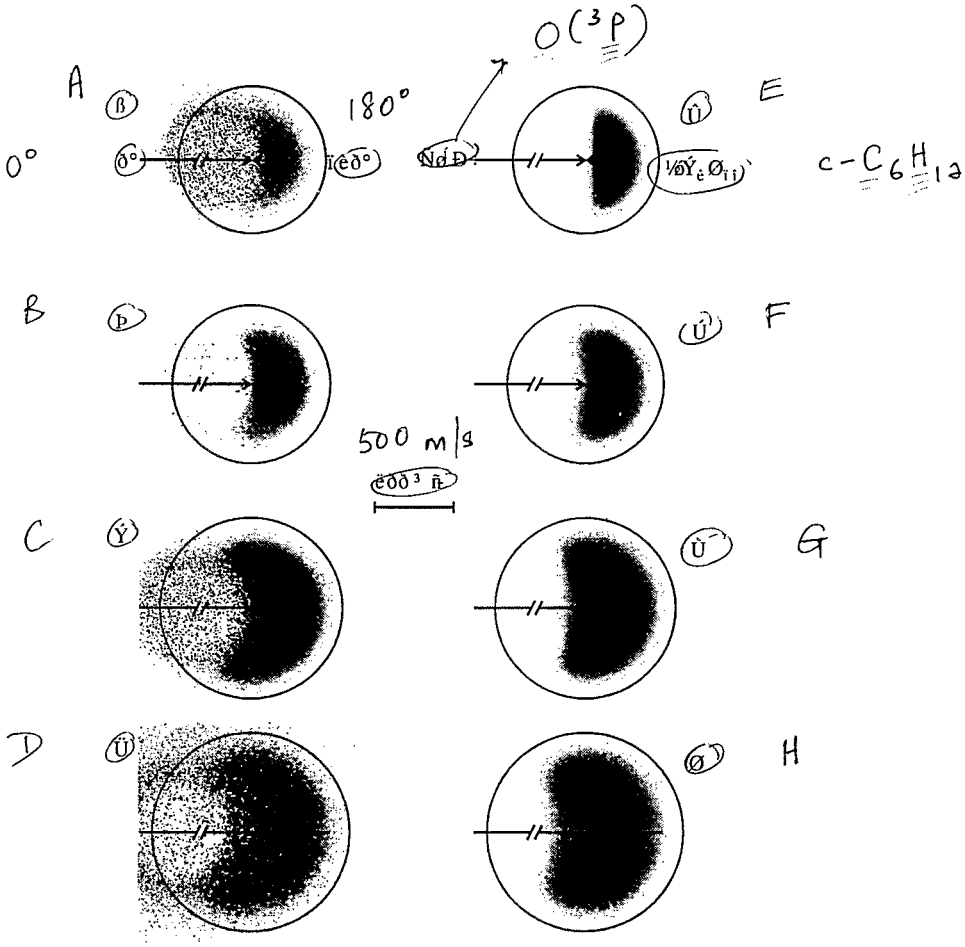


**Fig. 7.** Raw images (left column) and simulation images (right column) of the *c*-$C_6H_{11}$ radical from $O(^3P)$ + *c*-$C_6H_{12}$ reaction at collision energies of 4.7, 6.6, 11.3, and 14.8 kcal/mol (from A to D). Superimposed on the images are the velocity of the reactant and a ring showing the speed limit.

column of Fig. 7. These collision energies are the average of reactive collisions (obtained from the simulations), and are slightly higher (~0.5–1.0 kcal/mol) than the most probable collision energies since the collision energy distributions are broadened to higher energy. The photochemistry background has already been subtracted. Forward convolution fitting was performed only to one side of the image, owing to concerns about the detector performance, and the simulated images are shown in the right column of Fig. 7. The angular and translational energy distributions derived from the

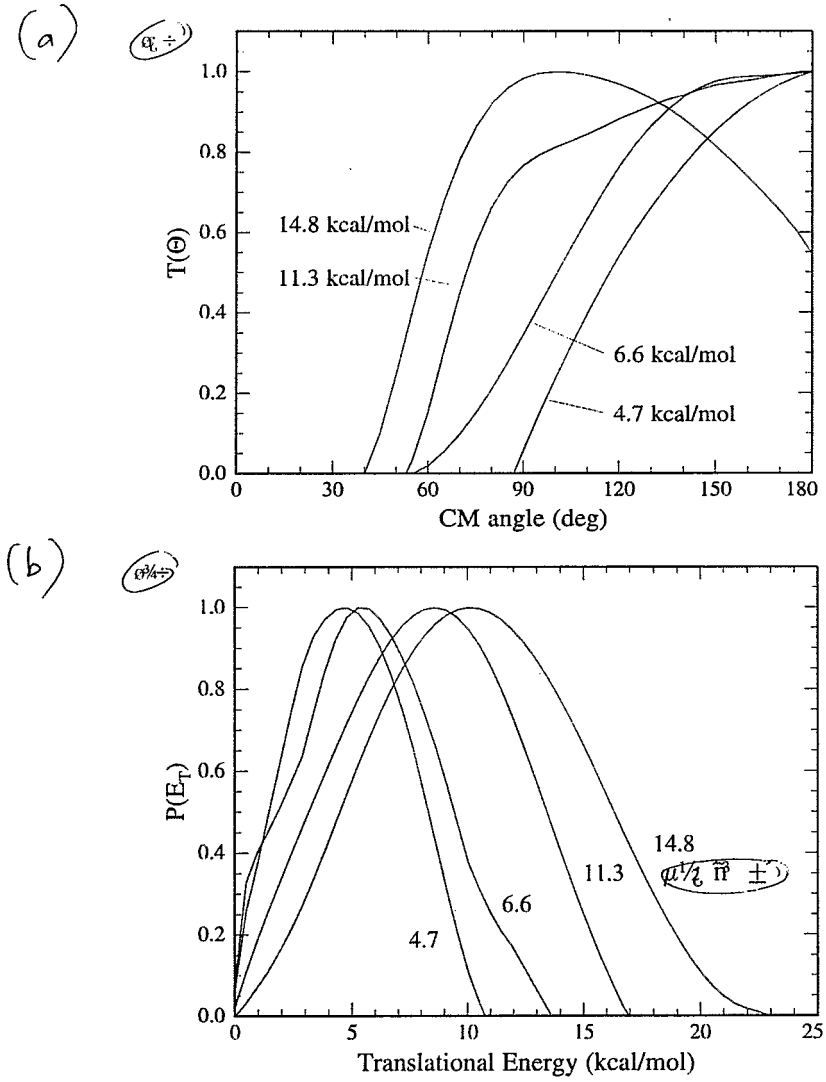


kcal/mol

**Fig. 8.** Angular (a) and translational energy (b) distributions for $O(^3P)$ + $c$-$C_6H_{12}$ reaction at different collision energies, derived from the images shown in Fig. 7.

images are shown in Figs. 8(a) and 8(b), respectively. It is evident that all images show clear backward-sideways scattering, and this backscattering angular distribution expands toward the forward direction with increasing collision energy. At the highest energy, the peak of the angular distribution actually moves away from the backward direction, peaking near 100°.

Table 2. Collision and translational energy parameters for indicated reactions (kcal/mol). $\langle E_{\rm coll}\rangle$ is the average collision energy for reactive collisions (see text); $\delta E_{\rm coll}$ is the FWHM spread in the collision energy; $E_{\rm avl}$ is the total available energy for the reaction; $\langle E_{\rm tr}\rangle$ is the average energy appearing in translation; $f_{\rm t}$ is the fraction of the total available energy appearing in translation; and $E_{{\rm int},R}$ is the energy in internal modes of the alkyl radical, given the OH vibrational excitation reported in Ref. 50.

| Alkane | $\langle E_{\rm coll}\rangle$ | $\delta E_{\rm coll}$ | $E_{\rm avl}$ | $\langle E_{\rm tr}\rangle$ | $f_{\rm t}$ | $E_{{\rm int},R}$ |
|---|---|---|---|---|---|---|
| Cyclohexane | 4.7 | 0.7 | 12.3 | 4.9 | 0.40 | 4.9 |
| | 6.6 | 1.0 | 14.2 | 5.9 | 0.42 | 5.2 |
| | 11.3 | 1.8 | 19.0 | 8.3 | 0.44 | 8.2 |
| | 14.8 | 2.5 | 20.1 | 10.5 | 0.47 | 9.9 |
| $n$-butane | 10.2 | 1.3 | 17.8 | 6.5 | 0.37 | 8.3 |
| isobutane | 10.2 | 1.3 | 20.2 | 7.8 | 0.39 | 7.5 |

The translational energy distributions peak at 30–40% of the available energy, and generally span from 0 to the limit of the available energy. Table 2 shows the average energy in translation and the average internal energy inferred in the alkyl product based upon Andresen and Luntz's values for the OH internal energy.

Shown in Fig. 9 are a set of images acquired for reactions of $O(^3P)$ with cyclohexane, ***n*-butane** and isobutane at the same 23 μs delay between the photolysis and probe lasers, and the corresponding simulation images. The collision energies are 11.3, 10.2 and 10.2 kcal/mol, respectively. The translational energy and angular distributions derived from the images are shown in Fig. 10. The angular distributions turn out to be very similar for all three reactions. The energy release parameters are also listed in Table 2 for comparison.

These results represent the first global differential cross section measurements for reactions of oxygen atom with alkanes. The angular distribution of broad backscattering we observe is actually a long anticipated result, and it was predicted in the original theoretical investigation by Luntz and Andresen using a semiempirical triatomic LEPS surface.[51] The distributions are quite similar to the H atom abstraction results for Cl + alcohols[26] reactions in Sec. 4, and also reminiscent of the backscattering component in the reactions of Cl + alkanes reported by Blank[18] *et al.* and Hemmi and Suits[19] (see Sec. 3). All of these reactions proceed over a barrier, although the barriers are much lower in the Cl case. The tendency of the angular distribution to extend to forward direction with increasing collision energy can also be readily understood for such rebound dynamics, because the

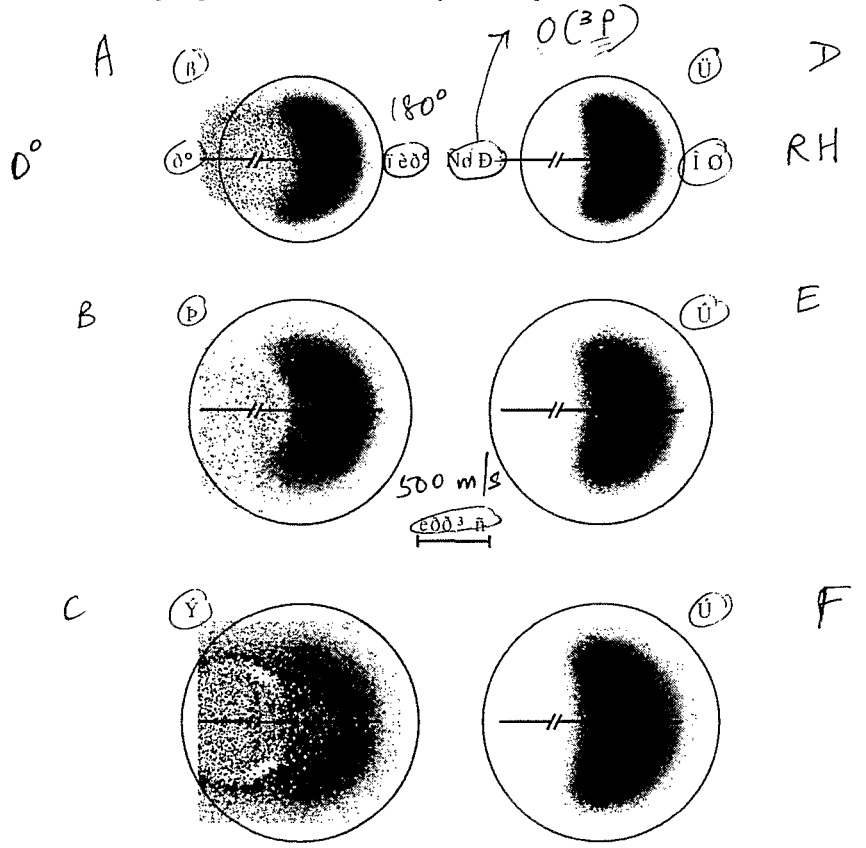


**Fig. 9.** Raw images (left column) and simulation images (right column) of the corresponding alkyl radicals from reactions of $O(^3P)$ with $c$-$C_6H_{12}$ at 11.3 kcal/mol (A,D), with n-butane at 10.2 kcal/mol (B,E), and with isobutane at 10.2 kcal/mol (C,F). Superimposed on the images are the velocity of the reactant and a ring showing the speed limit.

deflection at a given impact parameter tends to decrease with increasing collision energy and that, with higher collision energy, larger impact parameters may contribute to reaction in the "line-of-centers" picture[20] and thus enhance the scattering in the more forward direction. The tendency to move to sideways scattering at high collision energy, as we see in the result for cyclohexane at 14.8 kcal/mol collision energy, has also been seen in the Cl + propane reactions. It likely reflects the fact that the maximum in the opacity function does not occur at zero impact parameter *for the collision.* The opacity function in terms of a "local impact parameter" for the three atoms most relevant in the reaction, i.e. O–H–C, may peak at zero, but

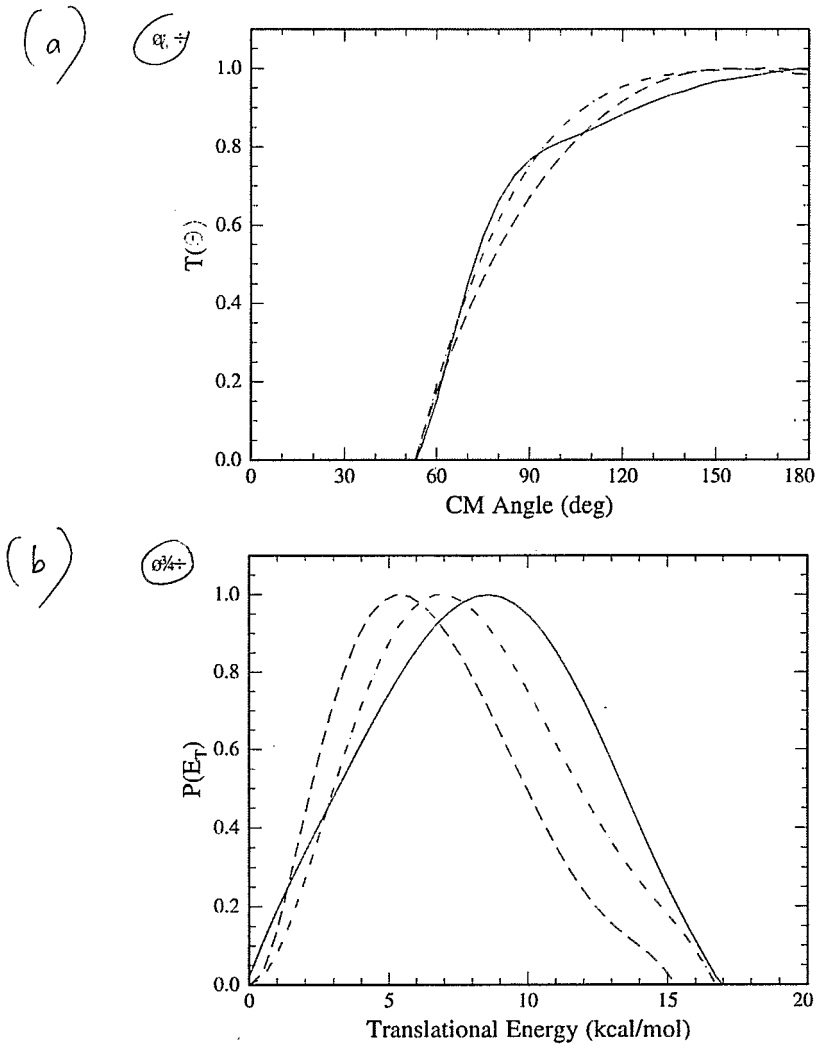


**Fig. 10.** Comparison of the angular (a) and translational energy (b) distributions for the reactions of $O(^3P)$ with $c$-$C_6H_{12}$, $n$-butane, and isobutane at collision energies of 11.3, 10.2, and 10.2 kcal/mol respectively, derived from the images shown in Fig. 9.

this is not likely to be zero for the genuine impact parameter in the overall collision frame. These important issues clearly distinguish model triatomic reaction dynamics from that of more complex polyatomic systems, and represent an area where theoretical modeling would provide valuable insight. It should be pointed out that the theoretical modeling we need here is

somewhat different from Valentini's local impact parameter model, which is aimed at understanding the $H_2$ (HA) product rovibrational distribution.

We notice a remarkable discrepancy between the angular distributions we observe and the results reported by Kajimoto *et al.*[55] They have obtained the differential cross section for OH ($v = 1$) product from $O(^3P)$ reaction with cyclohexane and isobutane obtained using Doppler-resolved, polarized laser-induced fluorescence spectroscopy under bulb conditions. Their angular distributions showed backscattering at their lowest collision energy, but the distributions become nearly forward-backward symmetric at high collision energy, and they proposed the onset of a stripping pathway to explain this phenomenon. Obviously, our angular distribution at similar collision energy disagrees with their higher collision energy case. Despite considerable effort, we were not able to find a satisfactory explanation for this substantial difference, which cannot be attributed to ambiguities in the data analysis of either experiment. The most significant difference between reaction conditions in the two experiments is the internal energy (and angular momentum) of the alkane reactant, although we have no good explanation of how this difference could lead to a substantial change in the angular distribution.

From the translational energy distributions we obtained and the result of very low OH internal energy from previous studies, we can obtain the alkyl product internal energy distribution. It is clear from the distributions and the parameters summarized in Table 2 that a remarkably large fraction of energy is partitioned into internal modes of the alkyl radical, regardless of the identity of the alkane reagent. This is somewhat surprising because the simple triatomic model has long been used to successfully explain the OH rotational excitation previously observed, which by definition assumes no internal energy in the alkyl radical product. In fact, in extracting the vibrational branching ratios from their LIF data, Andresen and Luntz,[50] as well as Whitehead[66] and others have assumed the alkyl co-fragment is completely cold. Some such assumption is necessary in order to account for the density-to-flux transformation in converting the measured LIF signals into populations. Both Andresen and Luntz, and Whitehead *et al.* estimated the sensitivity of their measured vibrational populations to these assumptions, and anticipated a deviation of 10–15% in the reported vibrational branching if 50% of the available energy were in fact partitioned to the alkyl radical. This modest correction will clearly not have a significant impact on the conclusions of these studies. Kajimoto and coworkers provided evidence for internal energy in the alkyl fragment in their Doppler

studies discussed above,[55] and noted that the simple triatomic picture of the reaction could not account for this. Unfortunately, their report only concerned the products formed in conjunction with OH ($v = 1$) so that it was difficult to generalize this aspect of their conclusions to the global dynamics.

The consensus, based upon an abundance of LIF spectra for many systems, has been that reaction proceeds through a collinear transition state, and this is reflected in the cold OH rotational distributions. The angular distribution, in the triatomic picture, was expected to show direct backscattering consistent with rebound reaction dynamics. The trends in the vibrational partitioning also fit perfectly into a collinear triatomic view. The finding of substantial internal energy in the alkyl product thus put forth a couple of questions: How can this quasi-triatomic picture be so successful at modeling the OH rotational and vibrational distributions and, at least roughly, the angular distribution, while more than 40% of the available energy ends up in internal modes of the polyatomic co-fragment? Since it is a direct rebound reaction, how does the polyatomic co-fragment get excited? These same questions apply to the Cl + alkane and Cl + alcohol results, which also showed substantial internal energy in the backscattered alkyl and hydroxyalkyl radical products. We propose a view of the reaction in which the H transfer is a "vertical" rather than "adiabatic" process, which suggests that, while the H atom is abstracted, the alkyl radical product is left with the same geometry as in its parent alkane, and its relaxation afterwards accounts for the major part of its internal excitation. This view is equivalent to the Franck–Condon picture often invoked to understand vibrational partitioning in photodissociation. Our *ab initio* calculations of the relaxation energy support this picture. The calculations are performed using the MOLPRO 2002 package[67] at the RCCSD(T) level with a cc-pVDZ basis set. To date, we have only finished for the case of *n*-butane. The relaxation energy is found to be 5.6 kcal/mol. This is indeed the magnitude we are looking for to account for the paradoxical success of the triatomic picture despite the large internal excitation. The last column in Table 2, showing the energy inferred in the alkyl radical assuming the OH vibrational excitation reported in Ref. 50, shows substantial support for this view. For the lowest collision energies in cyclohexane, we find 4.9 kcal/mol in internal degrees of freedom. As the collision energy is increased to 6.6 kcal/mol, at first there is little change in the internal excitation, increasing to only 5.2 kcal/mol. As the collision energy is further

increased, we begin to see more energy in the alkyl radical. This may be evidence of rotational excitation, or perhaps indication of additional excitation of vibrational modes of the radical. The question of rotational excitation in the alkyl radical is more difficult to address directly (ref JCP), and we are not going to the details here.

The differential cross sections for isobutane, the tertiary H abstraction case, are remarkably similar to the *n*-butane result. According to previous studies of this reaction by Andresen and Luntz and others, the vibrational excitation of the OH product is significantly greater for tertiary H atom abstraction, which has been ascribed to a change in the location of the saddle point closer to the reactants. It appears from the results here, summarized in Fig. 10 and Table 2, that this has little effect on the energy disposition in the alkyl radical co-fragment.

We thus need a revision of the triatomic picture to account for the dynamics of these reactions beyond the internal energy of the OH product. To a first approximation, the revision is to simply reduce the effective exoergicity by the relaxation energy of the alkyl radical product, ~5 kcal/mol. Then, we still anticipate conservation of translational energy and cold OH rotational distributions, the trends for OH vibrational excitation still depend only on the potential as a function of the C–H and H–O distances, but the internal energy of the product polyatomic radical is largely predetermined by the geometry of the parent hydrocarbon. Of course this picture only reproduces the broad features of the dynamics we observe. In fact, the translational energy distributions extend to the limit of the available energy, clearly showing that in some cases this relaxation energy in the radical can couple to translation.

Similar dynamics were observed in other H abstraction reactions (see Secs. 3 and 4). The Cl + alcohol reactions studied by Ahmed *et al.* showed dominant backscattering and ~35–40% of the available energy in translation. Blank *et al.* reported for Cl + propane reaction that there is a significant backscattered component showing substantial internal excitation in the propyl radical. We suspect a similar picture of "vertical" H atom transition may account for much of this, although the details will need to be modified by the different relaxation energies and barriers, etc. Nevertheless it seems reasonable to suggest, unless the timescale of the collision is very slow, this "vertical" reaction mechanism may be a normative principle for H abstraction dynamics in polyatomic molecules.

## 6 Concluding Remarks

The reaction dynamics of H atom abstraction from polyatomic molecules by H, Cl, and O atoms have so far been extensively investigated. Most of the studies have based on probing the diatomic product using REMPI or LIF approaches, while some recent studies probed the polyatomic product using VUV single photon ionization. There have been extensive measurements of the internal energy distribution of the diatomic product, and the measurement of the differential cross section is relatively rare. The reaction usually proceeds over a barrier with a collinear transition geometry, and the products are essentially backward scattered. With increasing collision energy and/or certain internal excitation of the polyatomic reactant, the acceptance cone is widened and the product angular distribution broadened.

Based on their extensive studies of the H + HX/HR reactions, Valentini's group has developed some simple models to understand the dynamics and its dependence on the HX/HR reactant, mainly focusing on the rovibrational distribution of the $H_2$ product. Owing to the complexity of the HR molecules, they tried to understand and predict the dynamics from the aspects of kinematics, thermochemistry, and the structure of HR. The main points includes the kinematic constraint on the product translational energy, truncation of large local impact parameter due to the competition of neighboring H atoms, and the relaxation of the coupling between the confinements of energy conservation and angular momentum conservation due to the presence of the polyatomic product as a energy-wise "cheap" sink of angular momentum.

Valentini's group recently developed a kinematic model to understand the energy partition in H-atom abstraction reaction, and the main conclusion is that there exists a lower limit to the kinetic energy release, or in other words there is an upper limit to the internal energy of the product that may be considerably lower than total available energy. This limit is related only to the mass combination in the reaction and the collision energy, effectively determined by the skew angle for the reaction. This model has successfully explained the rovibrational distribution of the diatomic $H_2$/HCl product measured in many H-atom abstraction reaction systems such as H + HCl, H + $C_6H_{14}$, and Cl + $C_2H_6$. However, this model fails to explain our translational energy release spectrum measurement for the O + alkane and Cl + alcohol reactions. It is surprising to note that Valentini and coworkers have not compared their model with any translational energy release spectra although the idea of the model is based directly on determination

of the lower limit of the translational energy of the reaction products. This is likely a consequence of the scarcity of such measurements until recently, and it highlights the importance of a global measurement of the dynamics. The main explanation for the failure of the model in the cases of O + alkane and Cl + alcohol reactions may be related to the invalidity of application of the collinear triatomic configuration in the model to the atom + polyatom systems, where there are many more degrees of freedom that can participate in the reaction.

With insight into the internal energy of the polyatomic product, which was made available by measurement of the translational energy release, we recently proposed a "vertical" H atom transition mechanism and modified the triatomic model to explain the global dynamics we observed for the O + alkane reactions. This mechanism may be a normative principle for H abstraction dynamics in polyatomic molecules. We expect more both experimental and theoretical dynamics studies in the future to help better understand the global dynamics, especially how the internal degrees of freedom of the polyatom play their roles in the reactions.

## Acknowledgments

This work was supported by the Director, Office of Energy Research, Office of Basic Energy Sciences, Chemical Sciences Division of the U. S. Department of Energy under contract No. DE-AC02-98CH10886. The authors wish to acknowledge the contributions of all who worked on these studies, and in particular Dr. M. Ahmed, D. S. Peterka and R. L. Gross for their efforts on the imaging studies.

## References

1. J. T. Herron and R. E. Huie, *J. Phys. Chem.* **73**, 3327 (1969).
2. J. T. Herron and R. E. Huie, *J. Phys. Chem. Ref. Data* **2**, 467 (1973).
3. J. T. Herron, *J. Phys. Chem. Ref. Data* **17**, 967 (1988).
4. R. Atkinson, D. L. Baulch, R. A. Cox, R. F. Hampson, J. A. Kerr and J. Troe, *J. Phys. Chem. Ref. Data* **21**, 1125 (1992).
5. C. A. Picconatto, A. Srivastava and J. J. Valentini, *J. Chem. Phys.* **114**, 4837 (2001).
6. A. Srivastava, C. A. Picconatto and J. J. Valentini, *J. Chem. Phys.* **115**, 2560 (2001).

7. G. J. Germann, Y.-D. Huh and J. J. Valentini, *J. Chem. Phys.* **96**, 5746 (1992).
8. P. M. Aker, G. J. Germann and J. J. Valentini, *J. Chem. Phys.* **90**, 4795 (1989).
9. G. J. Germann, Y.-D. Huh and J. J. Valentini, *J. Chem. Phys.* **96**, 1957 (1991).
10. P. M. Aker and J. J. Valentini, *Int. Rev. Phys. Chem.* **12**, 363 (1993).
11. P. M. Aker and J. J. Valentini, *Isr. J. Chem.* **30**, 157 (1990).
12. W. R. Simpson, T. P. Rakitzis, S. A. Kandel, T. Levon and R. N. Zare, *J. Phys. Chem.* **100**, 7938 (1996).
13. W. R. Simpson, T. P. Rakitzis, S. A. Kandel, A. J. Orrewing and R. N. Zare, *J. Chem. Phys.* **103**, 7313 (1995).
14. S. A. Kandel, T. P. Rakitzis, T. Levon and R. N. Zare, *J. Chem. Phys.* **105**, 7550 (1996).
15. D. F. Varley and P. J. Dagdigian, *Chem. Phys. Lett.* **255**, 393 (1996).
16. D. F. Varley and P. J. Dagdigian, *J. Phys. Chem.* **100**, 4365 (1996).
17. D. F. Varley and P. J. Dagdigian, *J. Phys. Chem.* **99**, 9843 (1995).
18. D. A. Blank, N. Hemmi, A. G. Suits and Y. T. Lee, *Chem. Phys.* **231**, 261 (1998).
19. N. Hemmi and A. G. Suits, *J. Chem. Phys.* **109**, 5338 (1998).
20. R. D. Levine and R. B. Bernstein, *Molecular Reaction Dynamics and Chemical Reactivity* (Oxford Univ. Press, New York, 1987).
21. Y. Yen, Z. Wang, B. Xue and B. Koplitz, *J. Phys. Chem.* **98**, 4 (1994).
22. M. Ahmed, D. S. Peterka and A. G. Suits, unpublished results.
23. S. H. Lee, L. H. Lai, K. P. Liu, and H. Chang, *J. Chem. Phys.* **110**, 8229 (1999).
24. K. Liu, (1999).
25. M. Ahmed, D. S. Peterka and A. G. Suits, *Chem. Phys. Lett.* **317**, 264 (2000).
26. M. Ahmed, D. S. Peterka and A. G. Suits, *PCCP Phys. Chem. Chem. Phys.* **2**, 861 (2000).
27. M. Ahmed, D. S. Peterka and A. G. Suits, *Chem. Phys. Lett.* **301**, 372 (1999).
28. M. Ahmed, D. Blunt, D. Chen and A. G. Suits, *J. Chem. Phys.* **106**, 7617 (1997).
29. P. A. Heimann, M. Koike, C. W. Hsu, D. Blank, X. M. Yang, A. G. Suits, Y. T. Lee, M. Evans, C. Y. Ng, C. Flaim and H. A. Padmore, *Rev. Sci. Instr.* **68**, 1945 (1997).

S. A. Nizkorodov, W. W. Harper, W. B. Chapman, B. W. Blackmon, and D. J. Nesbitt, *J. Chem. Phys.* **111**, 8404 (1999)

30. X. Yang, J. Lin, Y. T. Lee, D. A. Blank, A. G. Suits and A. M. Wodtke, *Rev. Sci. Instr.* **68**, 3317 (1997).
31. P. A. Willis, H. U. Stauffer, R. Z. Hinrichs and H. F. Davis, *J. Chem. Phys.* **108**, 2665 (1998).
32. P. A. Willis, H. U. Stauffer, R. Z. Hinrichs and H. F. Davis, *Rev. Sci. Instr.* **70**, 2606 (1999).
33. S. Arepalli, N. Presser, D. Robie and R. J. Gordon, *Chem. Phys. Lett.* **118**, 88 (1985).
34. S. G. Lias, J. E. Bartmess, J. F. Liebman, J. L. Holmes, R. D. Levin and W. G. Mallard, in *NIST Chemistry WebBook, NIST Standard Reference Database Number 69 (http://webbook.nist.gov)*, eds. by W. G. Mallard and P. J. Linstrom, National Institute of Standards and Technology, Gaithersburg MD, 1998.
35. S. Dobe, T. Berces, F. Temps, H. G. Wagner and H. Ziemer, in *Proceedings of the 25th Symposium (International) on Combustion*, Combustion Institute, Pittsburgh, 1994, p. 776.
36. B. Ruscic and J. Berkowitz, *J. Phys. Chem.* **97**, 11451 (1993).
37. B. Ruscic and J. Berkowitz, *J. Chem. Phys.* **95**, 4033 (1991).
38. J. M. Dyke, A. P. Groves, E. P. F. Lee and M. H. Z. Niavaran, *J. Phys. Chem.* **A101**, 373 (1997).
39. B. Ruscic and J. Berkowitz, *J. Chem. Phys.* **101**, 10936 (1994).
40. L. A. Curtiss, D. J. Lucas and J. A. Pople, *J. Chem. Phys.* **102**, 3292 (1995).
41. T. Khatoon, J. Edelbutteleinhaus, K. Hoyermann and H. G. Wagner, *Berichte Der Bunsen Gesellschaft Fur Physikalische Chemie* **93**, 626 (1989).
42. J. M. Williams and W. H. Hamill, *J. Chem. Phys.* **49**, 4467 (1968).
43. J. T. Jodkowski, M. T. Rayez, J. C. Rayez, T. Berces and S. Dobe, *J. Phys. Chem.* **A102**, 9219 (1998).
44. J. Edelbuttel-Einhaus, K. Hoyermann, G. Rohde and J. Seeba, in *Proceedings of the 24th Symposium (International) on Combustion*, Combustion Institute, Pittsburgh, 1992, p. 661.
45. X. Liu, R. L. Gross and A. G. Suits, *J. Chem. Phys.* **116** (2002).
46. X. Liu, R. L. Gross. G. E. Hall, J. T. Muckerman and A. G. Suits, *J. Chem. Phys.* **117**, 7947 (2002)
47. F. Ausfelder and K. G. McKendrick, *Progr. React. Kinet. Mech.* **25**, 299 (2000).
48. G. Paraskevopoulos and R. J. Cvetanovic, *J. Phys. Chem.* **81**, 2598 (1977).

49. R. F. W. Bader and R. A. Gangi, *J. Am. Chem. Soc.* **93**, 1831 (1971).
50. P. Andresen and A. C. Luntz, *J. Chem. Phys.* **72**, 5842 (1980).
51. A. C. Luntz and P. Andresen, *J. Chem. Phys.* **72**, 5851 (1980).
52. N. J. Dutton, I. W. Fletcher and J. C. Whitehead, *Molecular Physics* **52**, 475 (1984).
53. J. C. Whitehead and F. Winterbottom, *Chem. Phys. Lett.* **177**, 207 (1991).
54. G. M. Sweeney and K. G. McKendrick, *J. Chem. Phys.* **106**, 9182 (1997).
55. H. Tsurumaki, Y. Fujimura and O. Kajimoto, *J. Chem. Phys.* **112**, 8338 (2000).
56. T. Suzuki and E. Hirota, *J. Chem. Phys.* **98**, 2387 (1993).
57. S. P. Walch and T. H. Dunning, *J. Chem. Phys.* **72**, 3221 (1980).
58. D. W. Chandler and P. L. Houston, *J. Chem. Phys.* **87**, 1445 (1987).
59. A. Eppink and D. H. Parker, *Rev. Sci. Instrum.* **68**, 3477 (1997).
60. M. Kawasaki and H. Sato, *Chem. Phys. Lett.* **147**, 585 (1987).
61. P. Felder, C. S. Effenhauser, B. M. Haas and J. R. Huber, *Chem. Phys. Lett.* **148**, 417 (1988).
62. A. G. Suits, L. S. Bontuyan, P. L. Houston and B. J. Whitaker, *J. Chem. Phys.* **96**, 8618 (1992).
63. L. S. Bontuyan, A. G. Suits, P. L. Houston and B. J. Whitaker, *J. Phys. Chem.* **97**, 6342 (1993).
64. K. T. Lorenz, M. S. Westley and D. W. Chandler, in *Imaging in Chemical Dynamics*, eds. by A. G. Suits and R. E. Continetti, ACS, Washington D.C., 2001, p. 197.
65. G. C. McBane, in *Imaging in Chemical Dynamics*, eds. by A. G. Suits and R. E. Continetti, ACS, Washington D.C., 2000.
66. N. J. Dutton, I. W. Fletcher and J. C. Whitehead, *Mol. Phys.* **52**, 475 (1984).
67. R. D. Amos, A. Bernhardsson, A. Berning, P. Celani, D. L. Cooper, M. J. O. Deegan, A. J. Dobbyn, F. Eckert, C. Hampel, G. Hetzer, P. J. Knowles, T. Korona, R. Lindh, A. W. Lloyd, S. J. McNicholas, F. R. Manby, W. Meyer, M. E. Mura, A. Nicklass, P. Palmieri, R. Pitzer, G. Rauhut, M. Schutz, U. Schumann, H. Stoll, A. J. Stone, R. Tarroni, T. Thorsteinsson and H.-J. Werner, MOLPRO, a package of *ab initio* programs designed by H.-J. Werner and P.J. Knowles, version 2002.1